BASIC SPINTRONIC TRANSPORT PHENOMENA

Nicolas Locatelli[1,2] and Vincent Cros[2]

[1]Unité Mixte de Physique, CNRS, Thales, Univ. Paris-Sud, Université Paris-Saclay, 91767 Palaiseau, France

[2]Centre de Nanosciences et de Nanotechnologies, CNRS, Univ. Paris-Sud, Université Paris-Saclay, 91405 Orsay France

SPINTRONICS is a merger of magnetism and electronics. Conventional electronics uses only the charge of the electrons. For instance, transistors are based on the modulation of the density of electrons in a semiconductor channel by an electric field. Semiconductor-based memory (e.g., DRAM, Flash) stores information in the form of an amount of charge stored in a capacitor. In contrast, spintronics uses the spin of the electrons in addition to their charge to obtain new properties and use these properties in innovative devices. The spin of the electrons is an elementary magnetic moment carried by each electron. It has a quantum mechanical origin. Magnetic materials can be used as polarizers or analyzers for electron spins. This is why most spintronic devices combine magnetic and nonmagnetic materials, which can be metals, semiconductors, or insulators.

Magnetism has been used for a long time for data storage applications. Indeed, information can be stored in some magnetic materials in the form of a magnetization orientation. This was developed for storage on magnetic tapes as well as in magnetic hard disk drives (HDDs). The increase in the demand for storage capacity has stimulated an increase by eight orders of magnitude in the areal density of information stored in HDDs over the past 50 years; the bit area has decreased by the same factor. In 2014, bit sizes are typically on the order of $40\,nm \times 15\,nm$. This decrease in bit size has required continual improvements in the storage medium, in the write head used to switch the magnetization in the medium, and in the read head used to read out the magnetic state. This field of magnetic recording has benefited strongly from research and development in the field of spintronics. In particular, the discoveries of giant magnetoresistance in 1988 (1) and tunnel magnetoresistance at room temperature in

1995 (2,3) have been major breakthroughs from a scientific point of view, but they also helped recording technology keep moving forward. In 2010, a total of around 12,000 PB (10^{15} bytes) of storage capacity contained in 674.6 million HDDs were shipped worldwide.

Another type of spintronic devices that was proposed in the late 1990s is magnetic random-access memory (MRAM) (4). Indeed, solid state memory is of primary importance both for storage (the introduction of solid state drives in personal computers, tablets, and handheld devices) and for fast working memory between logic units and hard disk drives. In these applications, random-access memory based on devices involving magnetic materials, called magnetic tunnel junctions, are among the most promising technologies for future nonvolatile data storage, and may replace, in the near future, semiconductor-based memory (i.e., DRAM and SRAM), which represents a huge market.

This chapter is an introduction to the physical concepts required to understand how information is stored in a magnetic data cell, how this information can be detected, and how it is possible to modify the information by switching the magnetization from one state to another. First we introduce the basics of electronic transport in magnetic materials, a concept that is required for the comprehension of the physical mechanisms at the origin of magnetoresistive properties: giant magnetoresistance (GMR) and tunneling magnetoresistance (TMR), which is the magnetoresistive effect at play in spin-transfer torque (STT) MRAM devices. Then we describe how a spin-polarized current can exert a STT on the magnetizations in nanostructured spintronic devices by the interaction with local magnetic moments. Finally, we show how this novel effect can be used to modify the state of a magnetic element, leading to current-induced magnetization switching as the writing process in STT-MRAM.

1.1   GIANT MAGNETORESISTANCE

After introducing the basic concepts of electronic transport in ferromagnetic metals, a simple model of the GMR effect is presented, the so-called "two-current model" that was proposed to describe the dependence of the electrical resistance of magnetic multilayered stacks on their magnetic configuration. This model is helpful for the understanding of the basic principles of spin-dependent transport. Finally, the main applications of GMR are discussed.

1.1.1   Basics of Electronic Transport in Magnetic Materials

Magnetism, as produced by magnetite (Fe_3O_4), has been known from at least ancient Greek times. It was described as a force, either attractive or repulsive, that can act at distance. The origin of this force is due to a magnetic field that is created by some materials (called magnets), or is induced by the motion of electrons, that is, electrical currents. In magnetic materials, such as iron (Fe) or cobalt (Co), sources of magnetization are mainly the electrons' intrinsic magnetic moment associated with spin angular momentum, or simply "spin," and also to the electrons' orbital angular momentum. In Nature, other sources of magnetism are due to nuclear magnetic moments of the nuclei, typically thousands of times smaller than the

electrons' magnetic moments. Consequently, these nuclear moments are negligible in the context of the magnetization of materials. However, they play an important role in nuclear magnetic resonance (NMR) and magnetic resonance imaging (MRI).

The spin magnetic moment $\vec{\mu}_S$ and spin angular momentum $\vec{S}$ are linked through the relationship $\vec{\mu}_S = -g\mu_B\vec{S}$, where g is a dimensionless number called the g-factor (or Landé factor) and $\mu_B = e\hbar/2m_e$ is the Bohr magneton. In this expression, $e = 1.60 \times 10^{-19}$C is the electron charge, $m_e = 9.31 \times 10^{-31}$ kg is the electron mass, and $\hbar = 1.05 \times 10^{-34}$ m^2 kg/s is the reduced Planck constant. Due to the quantum mechanical nature of the spin, measurement of the projection of the electron spin $\vec{S}$ on any direction can take only two values: $+1/2$ and $-1/2$.

In the context of spintronics, the main question is to understand how this fundamental characteristic property of the electrons, that is, the spin, influences the mobility of the electrons in materials. In fact, although it was suggested by N. Mott in 1936, the influence of spin on the transport properties in a ferromagnetic material was clearly demonstrated experimentally and described theoretically only in the late 1960s (for a review, see Ref. 5). The property of spin-dependent transport is at the heart of not only the GMR effect but also all related effects that have allowed the development of spintronic devices.

The ferromagnetic transition metals, such as Fe, Co, Ni, and their alloys, which are the key compounds in today's spintronic devices, have a specific electronic band structure compared to normal (nonmagnetic) metals. In transition metals, the two highest filled energy bands, which are the conduction bands, are occupied by 3d and 4s electrons. This nomenclature refers to atomic orbitals of the electrons. They are labeled s-orbital, p-orbital, d-orbital, and f-orbital referring to orbitals with angular momentum quantum number l$=$0, 1, 2, and 3, respectively. These nomenclatures indicate the orbital shape and are used to describe the electron configuration. In a crystal, electrons with similar orbitals associate to fill a band of energy. More precise description on this topic can be found in any quantum mechanics textbook. In the case of ferromagnetic transition metals, each of these bands splits in two subbands corresponding to each spin configuration (see Fig. 1.1a). And in these magnetic materials, the interaction between spins, called the *exchange interaction*, energetically favors a parallel orientation of the electrons' spins.
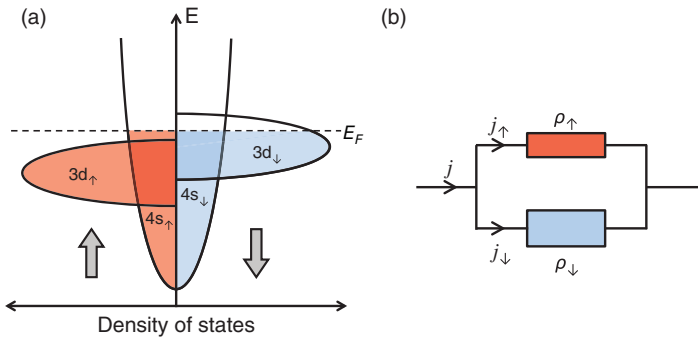
Figure 1.1   (a) Schematic representation of the band structure of a transition metal with strong ferromagnetic properties such as Co or Ni. (b) Equivalent circuit for the two-spin subbands in the "two-current" model.

In the following, we will refer to electrons with a magnetic moment aligned parallel to the local magnetization as "spin-up" (↑) electrons, and to electrons with a magnetic moment aligned antiparallel to the local magnetization as "spin-down" (↓) electrons.

As for ferromagnetic metals, similar to a normal metal, the 4s band contains almost an equal number of spin-up and spin-down electrons. But the specificity of ferromagnetic metals lies in the structure of their 3d bands, for which the resulting lowest energy situation corresponds to a shift of the two subbands $3d_\uparrow$ and $3d_\downarrow$ (Fig. 1.1a). This offset generates an asymmetry for the number of electrons of each orientation, also responsible for the spontaneous magnetization. Consequently, they are also known as majority spin (↑) and minority spin (↓) electrons. It finally creates, for each spin orientation, a difference between spin-up and spin-down densities of states at the Fermi energy E_F. We remind here that the density of states (DOS) $D(E)$ of a system describes the number of states $dn(E)$ per interval of energy dE around each energy level E that are available to be occupied by electrons: $dn(E) = D(E)dE$. The Fermi level E_F corresponds to the highest energy level occupied by electrons in a system at a temperature $T = 0$ K. Electrons involved in the transport process lie at (or close to) the Fermi level.

In the low-temperature limit, one considers that the electron's spin is conserved during most scattering events. Under this assumption, transport properties associated with spin-up and spin-down electrons can be represented by two independent parallel conduction channels (Fig. 1.1b), and the mixing of these two conduction channels is then considered as negligible. In ferromagnetic metals, these two channels have different resistivities $\rho_\uparrow$ and $\rho_\downarrow$, which depend on whether the electron magnetic moment is parallel (↑) or antiparallel (↓) to the direction of the local magnetization.

In a first, simple approximation, we can consider that 4s electrons, which are fully delocalized in the metal because they belong to outer electronic shells, constitute the conduction electrons that carry most of the current. In contrast, 3d electrons are more localized and responsible for the magnetic properties of the metal. The overlapping of s and d bands at the Fermi level allows current-carrying 4s electrons to be scattered on the localized 3d states, on the condition that they have the same energy and the same spin. The difference between the density of states of (↑) and (↓) 3d electrons at the Fermi level, therefore, results in different scattering probabilities for 4s electrons with spin (↑) or (↓).

In the case of Co and Ni, materials with strong magnetization, the bands are filled such that the Fermi level lies above the $3d_\uparrow$ subband. This subband is then completely filled and the $3d_\uparrow$ density of states at the Fermi level is zero (as illustrated in Fig. 1.1a). As a result, $s \rightarrow d$ electron scattering is possible only for s (↓) electrons, while (↑) electrons are not scattered on 3d states. This results in a much larger diffusion rate and thus a larger resistivity for the minority spin channel (↓) as compared to the majority spin channel (↑): $\rho_\uparrow < \rho_\downarrow$. At low temperature and under this approximation of two independent channels, the total resistivity of a ferromagnetic metal is then given by the following simple expression (6):

$$\rho = \frac{\rho_\uparrow \rho_\downarrow}{\rho_\uparrow + \rho_\downarrow}. \tag{1.1}$$

At high temperatures, some additional scattering of conduction electrons, for instance, by spin waves (propagating perturbations in the magnetic materials), can cause *spin-flip* events, that is, a mixing of the two conduction channels, but those can be ignored in first approximation up to room temperature.

Two definitions for the spin asymmetry coefficient of a given ferromagnetic material are used in the literature, $\alpha = \rho_\downarrow / \rho_\uparrow$ or $\beta = (\rho_\uparrow - \rho_\downarrow)/(\rho_\uparrow + \rho_\downarrow)$. In strong ferromagnets such as Co or Ni, $\rho_\uparrow < \rho_\downarrow$ and thus $\alpha > 1$.

A major consequence of the resistivity difference between conduction channels of minority and majority spin is that most of the current flows through the low resistivity spin ($\uparrow$) channel. Consequently, an asymmetry in the current densities associated with ($\uparrow$) and ($\downarrow$) electrons appears. Hence, the current flowing in the ferromagnetic material is *spin polarized*. Calling $j_\uparrow$ and $j_\downarrow$ the current densities of spin ($\uparrow$) and ($\downarrow$) electrons, respectively, and p the current spin polarization, p is defined by $p = (j_\uparrow - j_\downarrow)/(j_\uparrow + j_\downarrow)$. Note that $p = \beta$ at low temperature.
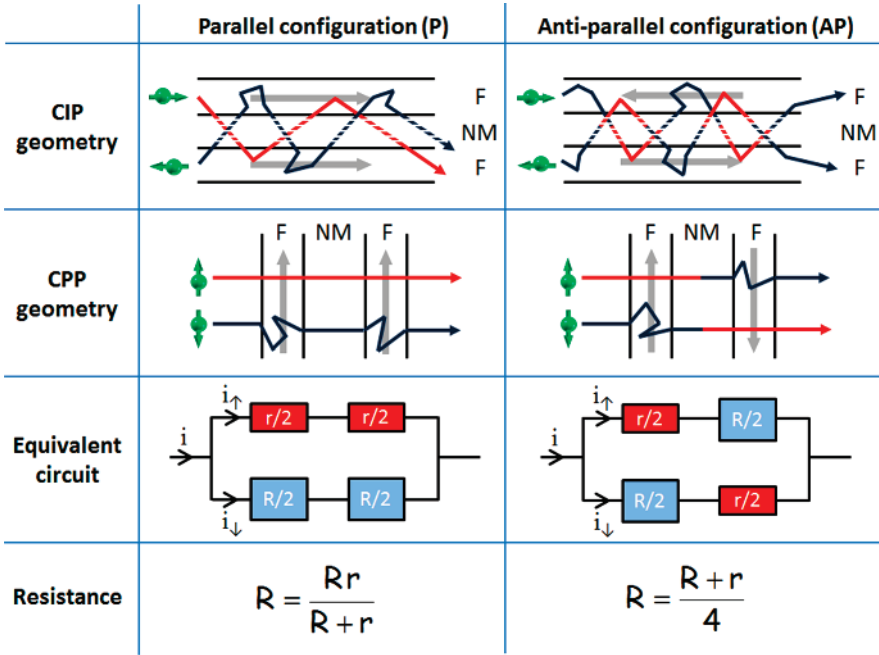
1.1.2   A Simple Model to Describe GMR: The "Two-Current Model"

Historically, the *two-current model*, proposed by Mott and then by Fert and Campbell, was developed to explain the spin-dependent resistivity in materials doped with magnetic impurities. It allows the anticipation, in a rather simple way, of the GMR effect in magnetic multilayers. For this, we consider an archetypal multilayered stack consisting of thin layers of alternating ferromagnetic metals (F) and nonmagnetic (NM) metals. The magnetization of the ferromagnetic layers is supposed to be uniform within each layer. We also assume that the relative orientation of the magnetization in the successive F layers can somehow be changed from parallel (*P*) to antiparallel (*AP*) magnetic configuration, as illustrated in Fig. 1.3. The way this is achieved will be explained in more detail in the next section.

Two geometries to evaluate the resistance of this multilayered structure can be considered: either with current flowing parallel to the plane of the layers (known as "current-in-plane GMR," CIP-GMR) or with current flowing in the direction perpendicular to the plane of the layers (known as "current-perpendicular-to-plane GMR," CPP-GMR). The same model can be used to evaluate the magnetoresistive properties for both geometries, provided that the layers' thickness remains small compared to a characteristic length associated with each geometry.

For the CIP case, the characteristic length is actually the mean free path λ. For the CPP case, it is the spin-flip length or spin diffusion length l_{sf} (7).

As illustrated in Fig. 1.2, during their Brownian motion throughout the structure with an average drift along the electrical field direction, the electrons traverse successive ferromagnetic layers. We denote $r/2$ the resistance associated with traversing a F layer for the majority spin channel (same direction as the magnetization) and $R/2$ the corresponding resistance for the minority spin channel (opposite direction to the magnetization), with $r < R$. $r/2$ and $R/2$ are associated with the average resistance sensed by the electrons as they spend half of their total path, respectively, in the majority or minority spin channels. For the sake of simplicity, let us also assume that the resistance of the nonmagnetic separating layer is much smaller

	Parallel configuration (P)	Anti-parallel configuration (AP)
CIP geometry		
CPP geometry		
Equivalent circuit		
Resistance	$R = \dfrac{Rr}{R+r}$	$R = \dfrac{R+r}{4}$

Figure 1.2   Illustration of the two-current model. The conduction paths of spin-up and spin-down electrons in a ferromagnetic metal/normal metal/ferromagnetic metal (F/N/F) multilayer, in the two cases of CIP and CPP transport. Conduction electrons with spin magnetic moment aligned antiparallel (blue paths) to the local magnetization experience more scattering events than those with parallel spin (red paths). The equivalent resistance circuit is represented for the two magnetic configurations: parallel and antiparallel.

than r and R. Then, in the *P* configuration, spin ($\uparrow$) and ($\downarrow$) electrons behave, respectively, as majority and minority electrons in all magnetic layers. As a result, the respective resistances of the two spin channels are $r_\uparrow = r$ and $r_\downarrow = R$. Since these two channels conduct the current in parallel, the equivalent resistance of the F/NM/F stack can be written as $r_P = rR/(r + R)$. In the case of materials with large spin asymmetry ($\alpha \gg 1$ and $r \ll R$), the multilayer can be considered short-circuited by the spin ($\uparrow$) channel; its equivalent resistance is $r_P \approx r$.

For the *AP* configuration, the electrons alternatively behave as majority or minority electrons as they propagate from one ferromagnetic layer to another. As a result, they are alternatively weakly and strongly scattered. Thus, the short-circuit effect previously mentioned in *P* configuration is here suppressed. In the *AP* configuration, the two channels have the same resistance $(R + r)/2$. The F/NM/F equivalent resistance is then $r_{AP} = (R + r)/4$, which is, in general, much larger than $r_P = r$.

Following this model, one can finally derive a simple expression for the amplitude of the GMR ratio:

$$\text{GMR} = \frac{r_{AP} - r_P}{r_P} = \frac{(R - r)^2}{4Rr}. \tag{1.2}$$

Let us mention that another definition of the GMR ratio is sometimes used in the literature, notably in theoretical articles. It consists of normalizing the resistance variation between P and AP configurations by the resistance in the AP configuration: $GMR = (r_{AP} - r_P)/r_{AP}$. In this definition, the GMR amplitude has a maximum value of 100%, whereas the commonly used definition often leads to magneto-resistive ratios over 100%. The GMR ratio is of prime importance for the characterization of the resistance variation, which is measured to determine the magnetic state of the stack.

1.1.3 Discovery of GMR and Early GMR Developments

The characteristic length scale of spin-dependent diffusion in thin films is on the order of a few nanometers in magnetic materials and tens of nanometers in nonmagnetic materials. These numbers explain why it took almost 20 years between the first basic studies on spin-dependent transport carried out on magnetic alloys in the late 1960s and the GMR discovery. GMR could be observed only in multilayered stacks consisting of nanometer thick layers. The growth of such multilayers became possible in the 1980s, thanks to the development of a new growth technique adapted from semiconductor industry: molecular beam epitaxy (MBE). GMR was actually discovered in magnetic metallic multilayers consisting of alternating layers of iron and chromium (Fe/Cr). This discovery by Albert Fert in Orsay, France, and Peter Grünberg in Jülich, Germany, in 1988, consisted of a very large variation in the CIP electrical resistance of these stacks under the application of an external magnetic field. Due to an antiferromagnetic coupling that exists between the successive Fe layers across the Cr spacers, the magnetization in the successive Fe layers spontaneously orient themselves in an AP configuration in zero magnetic field, as represented in Fig. 1.3. Upon application of a large enough magnetic field to overcome this antiferromagnetic coupling, the magnetization of all Fe layers can be saturated in the direction of the field, resulting in a P magnetic configuration. The GMR consists in a very large drop of resistance of 80% at 4 K (50% at 300 K) between the AP and P configurations. In 1988, it has been named "giant magnetoresistance" because the GMR amplitude was much larger than all known magnetoresistance effects at room temperature at that time. This discovery of GMR is considered the starting point of spinelectronics or spintronics. Almost immediately, GMR attracted enormous interest both from the point of view of fundamental physics and also for its possible applications, especially in the fields of data storage and magnetic field sensors. Fert and Grünberg were awarded the Nobel Prize in Physics in 2007 for this discovery.

Research on magnetic multilayers and GMR rapidly became a very active topic. It is not our aim here to provide an exhaustive review of all experimental and theoretical results that followed the initial discovery. A more complete review can be found in Ref. 6. Here we will rather introduce some of the key advances in GMR that occurred in the first years of spintronics.

Parkin et al. first demonstrated in 1990 the existence of GMR in multilayers prepared by sputtering (8), a simpler and faster physical vapor deposition (PVD) technique: a technique that is compatible with industrial processes. In magnetic multilayers consisting of alternating ferromagnetic and nonmagnetic layers, they also demonstrated the existence of oscillations in the FM interlayer coupling across the
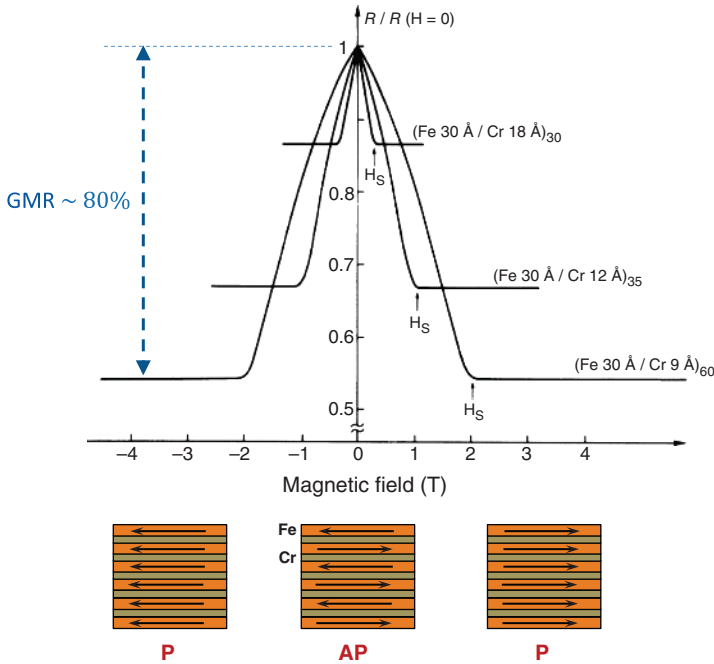
Figure 1.3   Normalized resistance as a function of external magnetic field $\mu_0 H$ for Fe/Cr multilayers, with different Cr intermediate layer thicknesses. The magnetic configuration is *AP* at zero external field and *P* at large applied fields (positive or negative). (Adapted from Ref. 1 with permission from American Physical Society.)

NM spacers as a function of the NM spacer thickness (see Chapter 2). This oscillatory coupling has been observed in a wide variety of multilayered systems, in particular (Fe/Cr) and (Co/Cu) multilayers. Another crucial step toward applications of GMR was also made in 1991 by Dieny et al., who developed trilayered ferromagnet/ nonmagnetic metal/ferromagnet (F/NM/F) structures called *spin valves*, which exhibit GMR at low magnetic fields (a few millitesla instead of a few teslas for (Fe/Cr) multilayers (9). In these trilayers, the magnetization of one of the ferromagnetic layers is pinned in a fixed direction using a phenomenon called exchange bias, whereas the magnetization of the second ferromagnetic layer can be easily switched in the direction of the applied field. It is then possible to change the magnetic configuration of these spin valves from *P* to *AP* by applying a weak magnetic field (a few millitesla) parallel or antiparallel to the direction of magnetization of the pinned layer. These systems, which exhibit very high 'resistance versus field' sensitivity, were introduced as magnetoresistive heads in hard disk drives by IBM in 1998.

1.1.4   Main Applications of GMR

GMR has been primarily used as spin-valve magnetoresistive heads in HDDs between 1998 and 2004. It was subsequently replaced by TMR heads, which exhibit even

larger magnetoresistance amplitude. GMR sensors are being used in other types of applications in the automotive industry, robotics, as three-dimensional position sensors, and sensors for biotechnological applications.

Some attempts have been made to use CIP-GMR for memory applications (MRAM), but only low-memory densities of about 1 Mbit per chip could be achieved. This memory is used mainly for space applications because of its radiation hardness (10).

1.2 TUNNELING MAGNETORESISTANCE

The development of artificial magnetic systems based on magnetic tunnel junctions (MTJs) was a second major breakthrough in spin electronics. Magnetic tunnel junctions look like spin valves from a magnetic point of view (two ferromagnetic layers separated by a nonmagnetic spacer) but a major difference is that the nonmagnetic spacer consists of a very thin insulating layer. In these junctions, the current flows perpendicular to the plane of the layers so that the electrons have to tunnel from one ferromagnetic layer to the other one across the thin insulating barrier.

After the pioneering work of Jullière (11) on Fe–GeO–Co junctions at 4.2 K in 1973, it was not until the mid-1990s that the improvement of both growth techniques and lithography processes allowed the fabrication of reliable MTJs. The devices studied used amorphous aluminum oxide (Al_2O_3) as the insulating barrier (2,3). They led to the first measurements of large magnetoresistive effects (TMR) with ratios on the order of 10–70% at room temperature. A great advantage of TMR with respect to GMR is the much larger impedance of MTJs compared to GMR metallic structures in the CPP geometry. Indeed, in MTJs, the resistance of the structure is effectively determined by the thickness of the tunnel barrier. MTJs can be patterned in the form of deeply submicrometer pillars with resistance ranging from kilohms to megohms, depending on the barrier thickness. This makes MTJs easier to integrate with CMOS components such as transistors, which have typical resistance in conducting mode of a few kilohms. In contrast, GMR submicrometer pillars in CPP geometry have resistances on the order of a few tens of ohms, which is fine for sensor applications, but difficult to integrate with CMOS components, in particular for MRAM applications.

An important research effort was undertaken on the materials side to improve the TMR amplitude. In 2004, it was discovered that much larger TMR ratios of about 250% at room temperature could be obtained in MTJs containing a monocrystalline magnesium oxide (MgO) barrier instead of an amorphous alumina barrier (12,13), reaching up to 600% at room temperature. These improvements have allowed a large increase of the sensitivity of magnetic HDD heads, which are needed for increased bit density. Thanks to their higher impedance than CPP-GMR devices, they also enabled new types of MRAM that could be scaled down in size and ramped up in density. Magnetic tunnel junctions are today the core elements of all MRAM technology (see Chapter 5).

As already mentioned, the transport mechanism across MTJs is no longer Ohmic transport as in GMR but relies on the well-known quantum mechanical tunneling effect. We start our second section by summarizing the basics of quantum

mechanical tunneling. This will allow us to introduce Jullière's model for TMR, giving an intuitive explanation of the magnetoresistive effect in magnetic tunnel junctions. This introduction will be completed by a description of a more accurate model (Slonczewski's model), and the spin filtering effect. Lastly, the important matter of voltage dependence of TMR will be discussed.

1.2.1   Basics of Quantum Mechanical Tunneling

In classical physics, charge transport through an insulating layer (even if it is ultra-thin) is forbidden. Hence, tunnel conduction through a potential barrier is a pure quantum mechanical phenomenon, called the *tunnel effect*. This effect, predicted in the early years of quantum physics, now has important applications in semiconductor devices such as the tunnel diodes. It is extensively described in elementary textbooks on quantum mechanics: we will only summarize here the main points relevant to MTJ physics.

In Fig. 1.4, the potential landscape for a (injector) metal–insulator–metal (collector) junction is schematically depicted. The main characteristics of the insulating barrier are its energy height Φ, and its thickness d. We consider an electron with an energy E, propagating in the metallic injector in the direction of the stack (perpendicular to the layers), with a wave vector amplitude $k_\perp = \sqrt{2m_e E / \hbar^2}$, where m_e is the electron effective mass and $\hbar$ is the reduced Planck constant. Based on the *free-electron approximation*, the resolution of Schrödinger's equation demonstrates that the electron has a nonzero probability of propagating through the insulating barrier and inside the collector electrode. We recall that in the free electron approximation, it is considered that the electrons are not subjected to any confining potential inside the metal or the barrier. The only potential variation is due to the insulating barrier. This model is well suited to $4s$ electrons, which are delocalized in the crystal.

Within the tunnel barrier, the electron wave function decays exponentially so that the probability for the electron to tunnel through the insulating barrier is given by
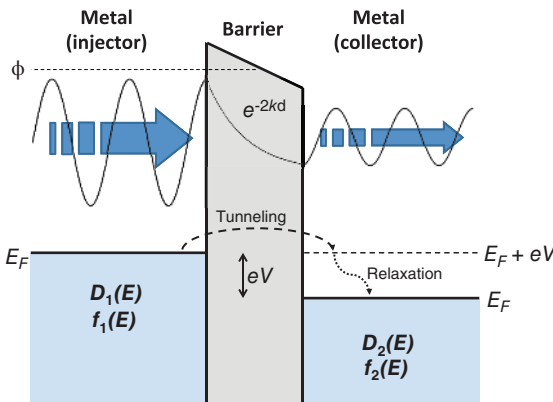
$$T(E) \propto e^{-2\kappa d}, \tag{1.3}$$

Figure 1.4   Schematics of the wave function of an electron tunneling between two metallic layers across a potential barrier.

with the decay coefficient $\kappa(E) = \sqrt{2m_e(\Phi - E)/\hbar^2}$. A first conclusion from these expressions is that in order to limit the MTJ resistance with typically used materials (MgO, Al_2O_3), the thickness of the insulating layer has to be on the order of a nanometer, corresponding to a few atomic layers. As an illustration, considering that an electron has to cross a $(\Phi - E_F) = 1$ eV barrier, it would experience a decay length of $1/\kappa \approx 0.2$ nm.

In MTJs at zero bias voltage, the Fermi levels of the two electrodes align so that the same number of electrons are steadily tunneling from one side of the barrier to the other and vice versa. In order to obtain a net nonzero current flow, a bias voltage has to be applied between the two metallic electrodes. When a bias voltage V is applied, the collector electrode's Fermi level is lowered by eV relative to the injector's, so that electrons tunnel from injector to collector (see Fig. 1.4). The resulting current then depends on the barrier properties, but also on the states accessible on both sides of the barrier. Indeed, according to the Fermi's golden rule, the probability for an electron having an energy E to tunnel through the barrier from metal 1 to metal 2 is proportional to the number of unoccupied electron states in 2 (collector) at this energy. In addition, the number of electrons that are candidates for tunneling is proportional to the number of occupied state in 1 (injector) at E. Therefore, the tunneling current from 1 to 2 due to electrons with energy E can be written as

$$I_{1\to2}(E) \propto D_1(E)f_1(E)\ T(E)\ D_2(E + eV)(1 - f_2(E + eV)),\qquad(1.4)$$

where $D_1(E)$ and $D_2(E + eV)$ are the density of states (DOS), respectively, in electrode 1 at the energy E and in electrode 2 at $(E + eV)$, and the functions $f_1(E)$ and $f_2(E)$ are the Fermi–Dirac distributions, which give the occupation probabilities of states in electrodes 1 and 2. Consequently, the product $D_1(E)f_1(E)$ represents the probability, in electrode 1, of having an electron with the energy E and $D_2(E + eV)(1 - f_2(E + eV))$ the probability, in electrode 2, of having an unoccupied state at the energy $(E + eV)$. Finally, the term $T(E)$ is the previously described transmission coefficient.

Using Eq. (1.4) to sum $I_{1\to2}(E) - I_{2\to1}(E)$ overall energies, the total tunneling current may be calculated. In the limit of zero temperature and small voltage V, it can be shown that only electrons at the Fermi level E_F contribute to the current. The resulting conductance is then simply proportional to the product of the densities of states at the Fermi energy in the two electrodes:
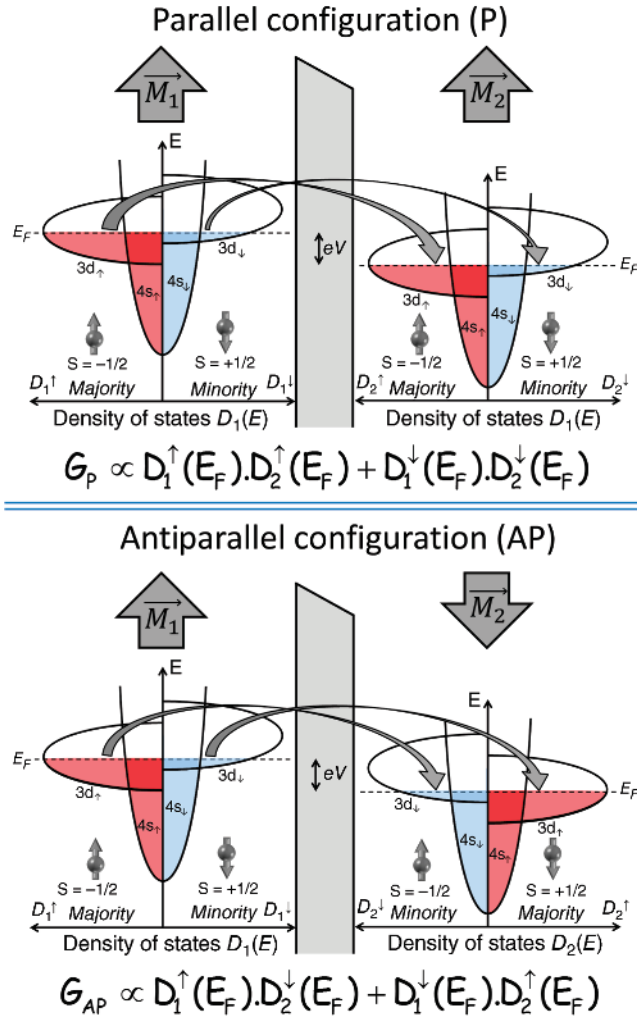
$$G_{T=0} \propto D_1(E_F) \cdot D_2(E_F).\qquad(1.5)$$

1.2.2 First Approach to Tunnel Magnetoresistance: Jullière's Model

The simplified approach described in the previous section for deriving the amplitude of the tunneling current was used by Jullière in 1975 to analyze his pioneer results of tunnel magnetoresistance in a MTJ composed of two ferromagnetic thin films, iron (Fe) and cobalt (Co), separated by a thin GeO semiconducting layer (11). The ferromagnetic character of the electrodes was taken into account by introducing different densities of states $D^\uparrow$ for the majority and $D^\downarrow$ for the minority electrons, using

the following definition for the spin polarization of a ferromagnet:

$$P_0 = \frac{D^\uparrow(E_F) - D^\downarrow(E_F)}{D^\uparrow(E_F) + D^\downarrow(E_F)}. \tag{1.6}$$

As for the GMR, the TMR can then be understood within the two-current model by summing in parallel the conductances of the spin-up and spin-down channels assuming that the tunneling process is spin-conserving. As illustrated in Fig. 1.5, in the P magnetic configuration, majority spin ($\uparrow$) electrons from the injector tunnel

Parallel configuration (P)

$$G_P \propto D_1^\uparrow(E_F).D_2^\uparrow(E_F) + D_1^\downarrow(E_F).D_2^\downarrow(E_F)$$

Antiparallel configuration (AP)

$$G_{AP} \propto D_1^\uparrow(E_F).D_2^\downarrow(E_F) + D_1^\downarrow(E_F).D_2^\uparrow(E_F)$$

Figure 1.5   Schematics of the spin-dependent tunneling process through an insulating barrier when the magnetizations in ferromagnetic electrodes are in parallel P or antiparallel AP magnetic configurations. The process is assumed to be purely ballistic, so that no mixing of spin states occurs during the tunneling process.

toward majority spin (↑) empty states in the collector. At the same time, minority spin (↓) electrons from the injector tunnel toward minority spin (↓) empty states in the collector. The conductance in P configuration is then written as

$$G_P \propto D_1^\uparrow(E_F).D_2^\uparrow(E_F) + D_1^\downarrow(E_F).D_2^\downarrow(E_F). \tag{1.7}$$

In case of AP magnetic configuration, majority spin (↑) electrons from the injector tunnel toward minority spin (↓) empty states of the collector. At the same time, minority spin (↓) electrons from the injector tunnel toward majority spin (↑) empty states of the collector. The conductance in AP configuration is then written as

$$G_{AP} \propto D_1^\uparrow(E_F).D_2^\downarrow(E_F) + D_1^\downarrow(E_F).D_2^\uparrow(E_F). \tag{1.8}$$

Using these expressions, the TMR ratio, which characterizes the resistance difference in P and AP configurations, may be expressed as

$$\text{TMR} = \frac{G_P - G_{AP}}{G_{AP}} = \frac{R_{AP} - R_P}{R_P} = \frac{2P_1P_2}{1 - P_1P_2}, \tag{1.9}$$

where $P_{1,2}$ are the spin polarization of electrode 1 and electrode 2 as defined in Eq. (1.6). Note that similar to the GMR case, a "pessimistic" definition of the TMR ratio can also be defined as $\text{TMR} = ((G_P - G_{AP})/G_P) < 1$.

   This model is oversimplified in the sense that it neglects all band structure effects in the magnetic electrodes and in the barrier. Nevertheless, this simple model successfully predicted the amplitude of TMR (typically around 50–70% with spin polarization on the order of 50–65% in Co–Fe-based alloys) in amorphous alumina-based magnetic tunnel junctions. However, the model failed to explain the very large TMR of magnetic tunnel junctions based on epitaxial barriers, notably of magnesium oxide (MgO) barriers. A key challenge to get an accurate prediction of TMR is to properly estimate the actual amplitude and sign of spin polarization for a given ferromagnetic material. Clearly, the larger the spin polarization, the higher the TMR amplitude. To maximize this spin polarization, a significant effort in materials science has been devoted to the search for half-metals, which are expected to be conducting for one spin direction and insulating for the other, resulting in 100% spin polarization at Fermi energy ($D^\downarrow(E_F) = 0$). Some magnetic oxides and Heusler alloys seem to exhibit this property in bulk form, but not when integrated in MTJs at room temperature.

   Several experimental techniques have been used to measure the ferromagnet's spin polarization, such as the Meservey and Tedrow technique (14), which is based on tunneling transport in FM–insulator–superconductor junctions. A list of typical values obtained for a variety of ferromagnetic materials is presented in Table 1.1.

   Other experiments in 1999, involving the study of spin-dependent tunneling through transition metal oxide barriers ($SrTiO_3$), revealed that different values and even opposite signs of spin polarization of tunneling electrons could be obtained for the same ferromagnetic electrode by varying the nature of the tunneling barrier (15).

TABLE 1.1 Values of Ferromagnet (FM) Spin Polarization P_0 Extracted from FM/Insulator/Al Tunneling Experiments, Where Al Is a Superconductor at Low Temperatures.

Ferromagnet	P_0 (%)
Ni	33
Co	42
Fe	45
$Ni_{90}Fe_{10}$	36
$Ni_{80}Fe_{20}$	48
$Co_{50}Fe_{50}$	51
$Ni_{40}Fe_{60}$	55

This technique of tunneling from a ferromagnet to a superconductor is used to determine the spin polarization in the ferromagnet (14).

These results clearly indicate that the spin polarization of the tunneling electrons is not only determined by the nature of the ferromagnetic electrodes but also by the whole trilayer ferromagnet/barrier/ferromagnet. In the following section, we introduce a more advanced model for treating the ferromagnet and the tunneling barrier configuration as a next step toward considering the whole trilayer band structure.

1.2.3 The Slonczewski Model

In 1989, Slonczewski proposed a more rigorous model based on the detailed calculations of the electron wave functions across the barrier, taking into account the exact matching conditions at the ferromagnetic/barrier and barrier/ferromagnetic interfaces (16). To derive the actual value of the transmission coefficient $T(E)$, one must consider not only the density of states of electrons at the Fermi level but also their wave vector k_F (or more simply their velocity v_F). This velocity is dependent on the type of electron one considers (s, p, and d bands). We will see below that this approach is required to understand the large values of TMR that are obtained in MgO-based MTJ devices.

1.2.3.1 The Model In Slonczewski model, several assumptions are made, similar to those of Jullière's model. First, the tunneling barrier is simply described as a square potential (energy height Φ and thickness d) above the Fermi level of the two ferromagnetic electrodes, considering the *free-electron approximation*. Second, the two ferromagnetic electrodes are taken to be identical. Finally, the model assumes that only electrons propagating perpendicular to the layers ($\vec{k} \approx \vec{k}_\perp$, $k_\parallel \approx 0$) can efficiently tunnel through the barrier. Indeed, if we consider electrons propagating in another direction, with $k_\parallel \neq 0$, then the decay coefficient inside the insulating layer becomes $\kappa(E) = \sqrt{k_\parallel^2 + \left(2m_e/\hbar^2\right)(\Phi - E)}$. Then, the higher the parallel wave vector, the lower the probability for the electron to tunnel through the barrier. By solving Schrödinger's equation in each part of the junction and applying continuity of the

wave functions at the interfaces, it was analytically demonstrated that the equivalent spin polarization of the ferromagnet/barrier couple, P, can be written as

$$P = \frac{\left(k_{F,\uparrow} - k_{F,\downarrow}\right)\left(\kappa^2 - k_{F,\uparrow}k_{F,\downarrow}\right)}{\left(k_{F,\uparrow} + k_{F,\downarrow}\right)\left(\kappa^2 + k_{F,\uparrow}k_{F,\downarrow}\right)} = P_0 \frac{\left(\kappa^2 - k_{F,\uparrow}k_{F,\downarrow}\right)}{\left(\kappa^2 + k_{F,\uparrow}k_{F,\downarrow}\right)}, \tag{1.10}$$

where $k_{F,\uparrow}$ and $k_{F,\downarrow}$ are the wave vectors for majority and minority electrons at the Fermi level, respectively, κ corresponds to the decay coefficient of the electrons' tunneling probability through the insulating barrier (see Eq. (1.3)), and P_0 corresponds to the previously defined polarization for a ferromagnet in Jullière's model (see Eq. (1.6)). Moreover, instead of defining a net polarization for the whole ferromagnetic layer, this expression highlights that the polarization actually depends on the type of electron one considers (to which band it belongs). Indeed, the values of κ, $k_{F,\uparrow}$, and $k_{F,\downarrow}$ are associated with the band one considers, and P can be derived for each of these bands.

The expression for the spin polarization P in this model reveals that the attenuation of the wave function while crossing the barrier also results in a decrease of the effective spin polarization of the total current. In the limit of large barrier height Φ, and hence large decay coefficient κ, the resulting polarization is equivalent to the one defined in the Jullière's model. This model emphasizes the importance of the electrons' properties in the calculation of the polarization. One can perform a simple calculation by considering only the contribution of the lighter (s band) electrons, but a more complete calculation would sum the contributions of each type of electrons.

1.2.3.2 Experimental Observations   On the experimental side, it has been noted that TMR amplitude varies considerably depending on the nature of the electrodes and the nature of the insulating barrier and interfaces. For example, Yuasa and Djayaprawira showed that in epitaxial magnetic tunnel junctions of Fe–Al_2O_3–CoFe, the TMR amplitude changes when the crystallographic orientation is changed among (211), (110), and (100) planes (17). The major role of the interfaces between the ferromagnet and the insulating layer has been highlighted by experiments demonstrating that Co/Al_2O_3 and Co/MgO provide positive polarization of tunneling electrons, whereas Co/$SrTiO_3$ provides negative polarization of tunneling electrons, at least at low bias voltage (15). These results demonstrate that it is possible to modify the TMR amplitude by choosing different ferromagnet/barrier configurations.

1.2.3.3 About the TMR Angular Dependence   Denoting θ the angle between the magnetization directions in the two ferromagnetic electrodes, Slonczewski also succeeded in deriving an expression of the tunnel conductance as a function of the angle θ in the limit of large potential barrier U:

$$G(\theta) = G_0\left(1 + P^2\cos\theta\right), \tag{1.11}$$

where the conductance in the *AP* configuration G_0 is given by

$$G_0 = \frac{\kappa}{\hbar d}\left[\frac{e\kappa\left(\kappa^2 + k_\uparrow k_\downarrow\right)\left(k_\uparrow + k_\downarrow\right)}{\pi\left(\kappa^2 + k_\uparrow^2\right)\left(\kappa^2 + k_\downarrow^2\right)}\right]^2 e^{-2\kappa d}, \tag{1.12}$$

which represents the actual conductance when the quantum system is considered as a whole (i.e., the two ferromagnetic layers separated by the tunnel barrier). With the effective tunnel conductance varying as $P^2\cos\theta$, the resistance dependence is then given by $R(\theta) = R_0/(1 + P^2\cos\theta)$, which can be approximated by $R \approx R_0(1 - P^2\cos\theta)$ when the electron polarization is weak, that is, for low TMR amplitude.

1.2.4   More Complex Models: The Spin Filtering Effect

Another major breakthrough in the field of spintronics was made with the discovery of much larger TMR amplitude in MTJ based on a crystalline MgO tunnel barrier rather than an amorphous alumina barrier. These MgO-based MTJs are today's standard elements in spintronic devices, whether for MRAM, read heads, or field sensors applications. The starting point of this work was the theoretical calculations carried out by Butler and Mathon in 2001, which predicted that TMR ratios as large as 1600% could be expected for epitaxially grown Co or Fe electrodes on MgO (18,19). For instance, an epitaxial MgO(001) barrier can be easily grown on a Fe bcc layer (001) since the lattice mismatch is small (about 4%). We remind that bcc stands for body-centered cubic, relative to the arrangement of atoms in the crystal. (001) later refers to a growth direction along the cube edge direction. These calculations, performed with *ab initio* methods, derived the tunneling probability of each kind of electrons, depending on their orbital symmetry.

1.2.4.1   *Incoherent Tunneling Through an Amorphous (Al₂O₃) Barrier*   The electrons' wave functions in crystalline materials are described by Bloch states. Bloch states are wave function solutions of the Schrödinger equation describing the quantum mechanical state of electrons in a periodic potential, for example, in a perfect, infinite atomic crystal. In crystalline ferromagnetic metals such as Fe, Ni, Co (3*d* ferromagnetic transition metals), and their alloys, these Bloch states have some specific symmetries: Δ_1 symmetry (corresponding to *spd* hybridized states), Δ_2 symmetry (*d* states), and Δ_5 symmetry (*pd* hybridized states). Bloch states with Δ_1 symmetry usually have a large positive associated polarization at E_F, but it is not the case for other symmetries (they can even have negative associated polarizations). Jullière's model (previously introduced) assumes equal tunneling probabilities independent of the electrons' Bloch states in the electrodes. This is true only if the tunneling process is *incoherent*, meaning that the coherency of the Bloch states is not conserved during tunneling.

In the case of an amorphous barrier, there is no crystallographic symmetry in the barrier. Consequently, electron wave functions from the injector, no matter their symmetry, couple identically to any *tunneling/evanescent states* in the barrier, through which they will propagate and decay. The exponential decay of the wave function throughout the barrier is then independent of the initial symmetry of the tunneling electron wave function so that the transmission probability through the barrier is itself independent on the initial electron wave function symmetry (see Fig. 1.6). This tunneling process can be regarded as an *incoherent tunneling*. It can be well described by Jullière's model introduced earlier. It leads to comparable tunneling
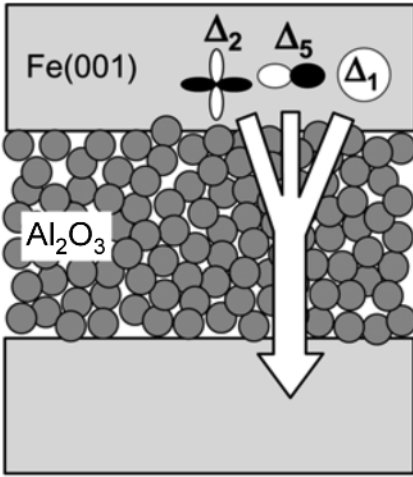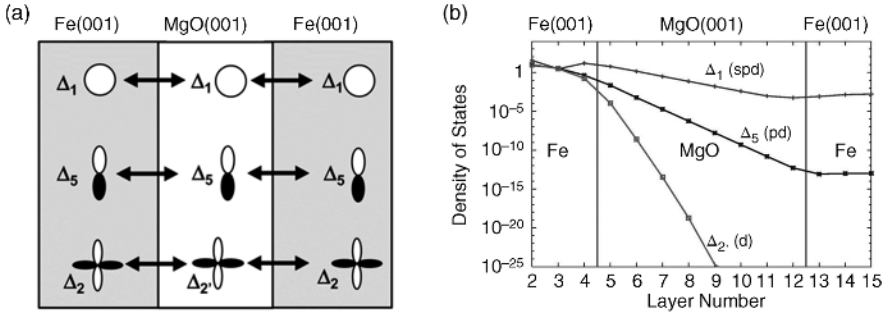
Figure 1.6   Schematic illustration of electrons tunneling through an amorphous (Al_2O_3) barrier. (From Ref. 17.)

probabilities for all Bloch states from the electrode. The *net* polarization then simply corresponds to the one calculated by summing the contributions from ($\uparrow$) and ($\downarrow$) DOS from all Bloch states. In this case, the net polarization is reduced due to the contributions of some Bloch states with negative spin polarization (i.e., opposite to the local magnetization).

A major difference between MTJ based on crystalline magnetic electrodes with amorphous barriers or crystalline barriers is that the symmetry of the tunneling electron wave functions may be conserved in the latter case and this symmetry can strongly influence the tunneling rates, that is, the probability of tunneling through the barrier. If one can engineer a system in which the Bloch states with large positive spin polarization have a higher tunneling probability than the Bloch states with negative spin polarization, then a very high net polarization could be expected, resulting in a very large MR ratio. This is possible in some epitaxially grown crystalline MTJs, in particular Fe/MgO/Fe, as explained in the following section.

1.2.4.2   *Coherent Tunneling Through a Crystalline MgO Barrier*

A crystalline MgO(001) can be epitaxially grown on a bcc Fe(001) layer to prepare a crystalline Fe(001)/MgO(001)/Fe(001) MTJ. Considering the $k_\parallel = 0$ direction, there are three kinds of tunneling/evanescent states in crystalline MgO, with different associated symmetries: Δ_1, $\Delta_{2'}$, and Δ_5. In such systems, *coherent* tunneling is obtained: The electrons' wave functions in the ferromagnetic material couple with evanescent wave functions having the same symmetry in the barrier, so that electrons conserve their orbital symmetry as they tunnel. *Ab initio* calculations then predict that the tunneling probability of an electron strongly depends on its orbital symmetry, leading to effective possible *symmetry filtering of the tunneling current*. The mechanism of orbital selection for the tunnel conductance in Fe(001)/MgO/Fe(001) systems is presented in Fig. 1.7a.

Figure 1.7   (a) Schematic illustration of the coupling between Bloch wave functions in iron and evanescent wave functions in MgO having the same symmetry. (Reproduced from Ref. 17 with permission from American Physical Society.) (b) Density of states for majority electrons tunneling ($k_\parallel = 0$) in a MTJ Fe(001)/MgO(001)/Fe(001) in the parallel magnetic configuration. Note the much slower decay of the DOS in the barrier for electrons with Δ_1 symmetry than for those of other symmetries. (From Ref. 17.)

In Fe, the band structure is calculated with consideration of the energy splitting between ($\uparrow$) and ($\downarrow$) for each Bloch state type, deducing the densities of states at the Fermi energy, and hence the polarization. Both majority and minority electrons fill many states at the Fermi energy, which corresponds to a small net polarization. But these calculations have demonstrated that only majority electrons fill Δ_1 symmetry states, implying a full polarization $P_{\Delta_1} = 1$, whereas both majority and minority Δ_2 and Δ_5 symmetry states can be found at the Fermi energy, corresponding to low polarizations. Note that for other materials such as bcc Co, only minority Δ_2 and Δ_5 symmetry states exist at the Fermi level, implying that $P_{\Delta_2} = P_{\Delta_5} = -1$.

Furthermore, calculations demonstrate that the exponential tunneling decay is much stronger for Δ_2 and Δ_5 states compared with Δ_1 states. Figure. 1.7b presents the probability for a majority electron incoming from the left electrode to propagate through the MTJ in the P configuration. For $d_{\text{MgO}} = 8$ monolayers (ML), which is a reasonable barrier thickness, the transmitted density of Δ_1 states is larger than that of Δ_5 states by 10 orders of magnitude.

In addition, since there are no minority $\Delta_{1\downarrow}$ states to tunnel from or to, only the $\Delta_{1\uparrow} \rightarrow \Delta_{1\uparrow}$ channel has a significant contribution to the conduction. Similarly, for the AP configuration, $\Delta_{1\uparrow} \rightarrow \Delta_{1\downarrow}$ and $\Delta_{1\downarrow} \rightarrow \Delta_{1\uparrow}$ channels have a potentially zero tunneling probability. There is therefore here a new mechanism of *spin filtering* of the wave functions according to their symmetry, which yields a dramatic effective increase in the net spin polarization of the tunneling current. As a result, significant conduction occurs only in the P configuration. It is this *spin filtering effect* that explains the very large TMR magnitudes predicted and measured in epitaxial or highly textured MgO-based MTJs.

Not only bcc Fe(001) shows this high spin polarization of the Δ_1 Bloch states, but also many other bcc ferromagnetic metals, such as cobalt (Co) and alloys based on Fe and Co. Similarly, very large TMR ratios are also predicted for other crystalline barriers such as $SrTiO_3$ (20). However, so far, MgO-based MTJs still give the best results in terms of TMR. After these theoretical predictions, a strong worldwide

research effort was made to obtain epitaxial growth of structures for Fe/MgO/Fe or CoFeB/MgO/CoFeB. These efforts resulted in an extremely large TMR of about 600% obtained in 2008 in CoFeB/MgO/CoFeB MTJs at room temperature (21). The difference between the values of experimental and theoretical TMR is mainly due to imperfections in interface quality and defects in crystal growth of materials due to dislocations, vacancies, and impurities (in particular absorbed water molecules). More details on the growth of MgO-based MTJs can be found in Chapter 2 as well as in Ref. 17.

1.2.5 Bias Dependence of Tunnel Magnetotransport

In most MTJs, the magnitude of TMR decreases markedly when the applied voltage increases. This factor is critical for applications and particularly for reading out the memory magnetic state in MRAM. This voltage-induced decrease of TMR in magnetic tunnel junctions is characterized by $V_{1/2}$, which is the voltage for which the TMR ratio is reduced to half of its amplitude in the limit of zero bias voltage. Several theories have been developed to describe this bias dependence of the magnetotransport, which is often very complex because it involves several physical mechanisms of spin depolarization, as explained below.

The first of these mechanisms is based on the emission of magnons by hot electrons. When a finite bias voltage is applied across the junction, the electrons tunnel ballistically through the barrier, that is, keeping their energy so that they arrive in the collector electrode as hot electrons (Fig. 1.4). When they penetrate the collector electrode, these hot electrons very quickly lose their excess energy by inelastic relaxation to the Fermi energy. In a normal metal, the relaxation mechanisms are via electron–electron and electron–phonon interactions. In ferromagnetic materials, electrons can also reach the Fermi energy by emission of spin waves (magnons), a process that does not preserve the spin. The higher the voltage, the greater the density of emitted magnons. Both the spin polarization of the current and the TMR, directly linked to the conservation of spin information, are then reduced.

Another mechanism of spin depolarization of the current is the presence of defects inside the insulating barrier. These defects create trap states in the barrier through which electrons can co-tunnel. This means that electrons tunnel from the injector to the trap, and then from the trap to the collector, losing their spin information in the process.

Finally, the decrease of TMR with bias voltage can be described by the voltage dependence of the electronic properties involved in the tunneling process, for example, the electron effective mass, the transmission coefficients in the barrier, and the parameter of coherent reflections at interfaces. The polarization of the tunneling electrons also depends itself on the bias voltage since at a bias voltage V, electrons within a band of width eV below the Fermi energy can tunnel through the barrier. If one considers a band structure such as the one depicted in Fig. 1.1a, it is clear that the net polarization of the tunneling electrons is expected to decrease if electrons from below the Fermi energy become allowed to tunnel through the barrier.

In MgO-based MTJs, $V_{1/2}$ is typically in the range of 0.5–0.8 V, depending on the nature of the magnetic electrodes and growth conditions. The readout in MRAMs

is usually performed at voltages on the order of only 0.15–0.2 V for which the drop of TMR is weak.

1.3 THE SPIN-TRANSFER PHENOMENON

In the first generation of MTJ-based MRAM, the switching of the storage layer magnetization during the write process is achieved using pulses of magnetic field (4). This field is induced by a current flowing in conducting lines located above and below the MTJ. This writing process suffers both from the large energy consumption needed to generate large enough magnetic fields and from write selectivity problems due to the spatial extension of generated fields as well as dot-to-dot distribution in switching fields (variability). A new generation of magnetic memory, called spin-transfer torque magnetic random-access memory (STT-MRAM), is based on the pioneering theoretical work of Slonczewski (22) and Berger (23), which predicted that current flowing through magnetic multilayers can directly reverse the magnetization of one of the layers.

We describe below the origin and consequences of this physical phenomenon. The details of the reversal dynamics as well as the use of this new writing mode in MRAM will be described in other chapters.

1.3.1 The Concept and Origin of the Spin-Transfer Effect

The GMR and TMR magnetoresistive effects described in the previous sections correspond to a variation of the current flow in a spin-valve device or a magnetic tunnel junction (i.e., a variation in conductance) induced by a change of the magnetic configuration of the device. This change of magnetic configuration was generally mediated through the action of an external field. The spin-transfer effect may be seen in a simple description as the reciprocal effect to GMR or TMR: via the spin-transfer torque, the current, which gets spin polarized by traversing a first magnetic layer, can exert a torque on the magnetization of a second ferromagnetic layer and thereby change the magnetic configuration of the device.

The simplest system for describing this new effect is similar to the standard magnetoresistive systems described in previous sections. It consists of two thin magnetic layers separated by a nonmagnetic layer (either a normal metal NM or an insulator I). One of the two ferromagnetic layers, F1 is presumably thick and fixed, whereas the second ferromagnetic layer F2 and the nonmagnetic one are chosen to be thin in comparison to the previously introduced characteristic length of spin-polarized transport.

1.3.1.1 The "In-Plane" Torque When electrons flow through the structure perpendicularly to the interfaces, the current spin polarization evolves to remain parallel to the direction of the local magnetization. Indeed, when the electrons penetrate into a ferromagnetic material, the spins of the conduction electrons become very rapidly aligned parallel to the local magnetization direction because of a strong exchange interaction between conducting electrons ($4s$) and the more localized electrons ($3d$) responsible for the local magnetization (see Section 1.1).
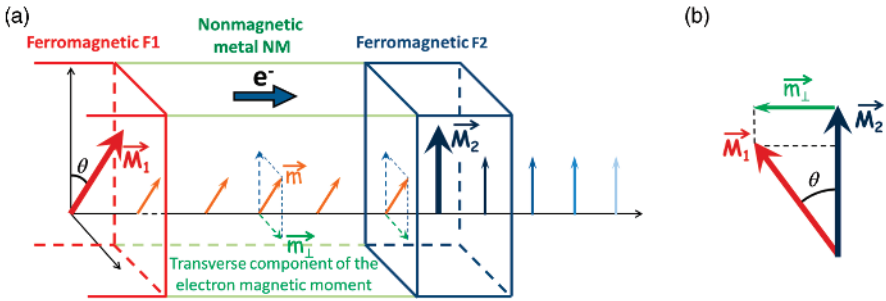
Figure 1.8 (a) Illustration of the concept of spin-transfer torque in a simple F1/NM/F2 trilayer structure; (b) Torque $\vec{m}_\perp$ exerted on the magnetization $\vec{M}_2$ of the thin magnetic layer F2, which tends to get aligned along the magnetization $\vec{M}_1$ when electrons flow from F1 to F2.

In the case where the respective magnetizations $\vec{M}_1$ and $\vec{M}_2$ are noncollinear, the spin polarization of electrons have to rotate in their paths. This occurs mainly through relaxation of the spins transverse component at the F/NM interfaces. We illustrate this phenomenon by considering the case of a spin-valve structure where the nonmagnetic spacer is metallic (NM) as illustrated in Fig. 1.8. When the electrons flow from layer F1 to F2, the current becomes spin polarized after traversing F1, through the mechanism described in Section 1.2 and thus acquires a net spin polarization along $\vec{M}_1$. This nonzero spin polarization propagates across the NM spacer as long as the spin-flip is negligible in this layer. The transmitted electrons then impinge on the NM/F2 interface with a spin polarization that is not aligned with the direction of the local magnetization $\vec{M}_2$.

If we focus on the relaxation process at the second NM/F2 interface, the incoming electrons hence have a component of their magnetic moment $\vec{m}$ transverse to the $\vec{M}_2$ direction (see Fig. 1.8a). When they penetrate into F2, their spin becomes quickly aligned toward the local magnetization direction in a very short distance after the interface (typically less than a nanometer). Hence, the electrons lose their transverse component $\vec{m}_\perp$ when they penetrate into F2 within the first nanometer from the interface. In this interaction however, the total spin angular momentum is conserved, and thus the transverse component $\vec{m}_\perp$ has been actually absorbed and transferred to the magnetization of F2.

This *transfer of spin* is therefore intrinsically an interfacial effect. For a very thick magnetic layer, with very stable magnetization, it then has a negligible influence. However, for a thin layer, this *transfer of spin* tends to modify the local magnetization direction, somehow adding the transferred spins to it. As a result, this *transfer of spin* tends to align the magnetization $\vec{M}_2$ along the direction of the spin current polarization, and hence along the magnetization $\vec{M}_1$ (see Fig. 1.9a) when electrons flow from the "reference" or "fixed" layer F1 to the "free" layer F2. It translates as a torque exerted on the magnetization $\vec{M}_2$, named *spin-transfer torque*.

If electrons now propagate in the opposite direction, that is, from layer F2 to layer F1, electrons impinging on the NM/F1 interface with spin antiparallel to the F2
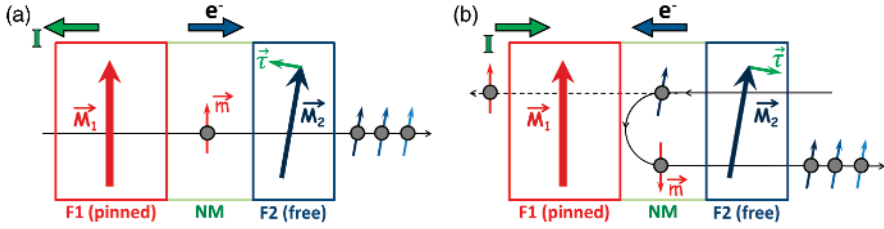
Figure 1.9   In a F1(pinned)/NM/F2(free) trilayer structure, illustration of the sign reversal of the spin-transfer torque with changing the current sign. (a) Positive current tends to align magnetization $\vec{M}_2$ parallel to $\vec{M}_1$. (b) Negative current tends to push $\vec{M}_2$ away from $\vec{M}_1$.

magnetization will have difficulty penetrating into the F1 layer or will be back-scattered because their spin is antiparallel to the local magnetization. These electrons are therefore reflected by the NM/F1 interface and impinge on the other side of the NM spacer on the NM/F2 interface with a spin antiparallel to the F1 magnetization. This flow of reflected electrons again exerts a torque on the F2 magnetization which now tends to align the F2 magnetization antiparallel to the F1 magnetization (see Fig. 1.9b). The STT therefore changes sign as a function of the current direction and can favor either *P* or *AP* magnetic configurations depending on its direction.

As the current density increases, the number of electrons crossing the magnetic layer per unit time increases, thereby proportionally increasing the spin-transfer torque. Therefore, in metallic spin valves, STT can be considered proportional to the current density.

If the system is a magnetic tunnel junction, as in STT-MRAM, the electrons are transmitted ballistically through the spacer layer (the tunnel barrier) instead of diffusely as in spin valves, but the STT effect is basically similar.

Analytically, the spin-transfer torque is equal to the sum of the absorbed transverse spin magnetic moments per unit time:

$$V \frac{d\vec{M}_2}{dt} = \text{absorbed transverse magnetic moments per unit time,} \qquad (1.13)$$

considering that each electron flowing across F2 will bring a contribution $\vec{m}_\perp$ to the local magnetization:

$$\vec{m}_\perp = -\frac{g\mu_B}{2} \left(\vec{m}_2 \times \left(\vec{m}_2 \times \vec{m}_1 \right) \right), \qquad (1.14)$$

In this formula, the cross product $-\left(\vec{m}_2 \times \left(\vec{m}_2 \times \vec{m}_1\right)\right)$ simply corresponds to the direction of the electron's transverse magnetic moment $\vec{m}_\perp$. The free layer volume is $V = t \cdot A$ (t the thickness, A the cross section), g is the electrons Landé factor, and μ_B is the Bohr magneton. The normalized magnetization is given by $\vec{m}_i = \vec{M}_i/M_{S_i}$, where M_S is the saturation magnetization. The number of incoming electrons per second is then simply given by

$$\frac{dN}{dt} = \frac{j_{dc} \cdot A}{e}, \qquad (1.15)$$

where j_{dc} is the injected current density and e the electron's charge. By summing the contributions, and considering the current spin polarization P_{spin} at the NM/F2 interface, one obtains the expression for the spin-transfer torque as

$$\left(\frac{d\vec{m}_2}{dt}\right)_{ST} = -P_{spin}\frac{j_{dc}}{2te}g\mu_B\left(\vec{m}_2 \times \left(\vec{m}_2 \times \vec{m}_1\right)\right). \tag{1.16}$$

This torque is often labeled "Slonczewski torque" (ST) or "in-plane torque" since its direction lies in the plane defined by $\vec{M}_1$ and $\vec{M}_2$. It is proportional to the current spin polarization at the interface, and to the current density. Hence, one can directly change the magnitude or even the sign of the effect by simply tuning these two parameters. Remarkably, by changing the sign of the current, it is possible to reverse the effect. One sign of the current will make the local magnetization $\vec{M}_2$ rotate to align along the magnetization $\vec{M}_1$ (thus favoring parallel magnetizations), while the other sign will make the local magnetization rotate away from the magnetization $\vec{M}_1$ (thus favoring antiparallel magnetizations). A review on in-plane torque in metallic spin valves can be found in Ref. 24.

1.3.1.2 The "Out-of-Plane" Torque   The in-plane torque is always the dominant spin-transfer effect in junctions, and is the most significant torque in all metallic structures. However, an additional component of spin-torque can also become significant in tunnel junctions. It is referred to as field-like torque (FLT) or out-of-plane torque, and is associated to another source of spin-transfer, leading to a torque directed perpendicular to the $\left(\vec{M}_1, \vec{M}_2\right)$ plane. Its action is equivalent to applying an external magnetic field oriented along the $\vec{M}_1$ direction. The physical phenomena behind the effect are beyond the scope of this book; we will simply mention that

$$\left(\frac{d\vec{m}_2}{dt}\right)_{\text{Out-of-plane}} \propto -\left(\vec{m}_2 \times \vec{m}_1\right). \tag{1.17}$$

This out-of-plane torque is often considered through its ratio to the in-plane torque. It is usually negligible in metallic spin valves but its amplitude can reach about 30% of the in-plane STT in tunnel junctions. It is often neglected in first approximation but nevertheless can be responsible for undesirable behavior in the writing operation of STT-MRAM such as back-switching phenomena (25).

1.3.2 Spin-Transfer-Induced Magnetization Dynamics

After having introduced the spin-dependent transport mechanisms at the origin of spin-transfer torques, our aim is now to address the influence of these torques on the magnetization dynamics of F2. The dynamics of a magnetization in response to external torques in a solid is classically described by the Landau-Lifshitz-Gilbert (LLG) equation. Because of the STT, two terms associated to the in-plane and out-of-plane components of spin-transfer torques are added to this equation. The LLG equation and the detailed description of magnetization dynamics are the topic of another chapter. Here, we describe only some phenomenological aspects.
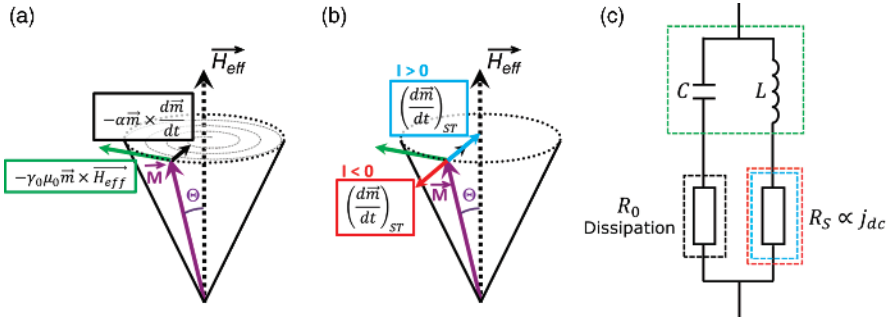
Figure 1.10 (a) Relaxation of magnetization around the effective field without spin-transfer torque. (b) Additional torque for positive or negative current. (c) Corresponding equivalent (RLC) circuit.

We return to the simple trilayer of Fig. 1.8 and consider the ferromagnetic layer F2, whose local magnetization is described by the normalized vector $\vec{m}_2$. This magnetization is aligned at equilibrium along the so-called effective field $\vec{H}_{eff}$. $\vec{H}_{eff}$ is the field resulting from the sum of all fields acting on $\vec{M}_2$, namely, the external applied magnetic field, magnetic anisotropy field, interlayer coupling field, and so on. When $\vec{M}_2$ is slightly pushed away from its stable equilibrium position, the magnetization starts precessing around the effective field $\vec{H}_{eff}$, following the differential equation:

$$\left(\frac{d\vec{m}_2}{dt}\right)_{precession} = -\gamma_0 \vec{m}_2 \times \mu_0 \vec{H}_{eff}, \tag{1.18}$$

where γ_0 is the gyromagnetic ratio and μ_0 is the vacuum permeability. Like any other physical system with a stable equilibrium position, the magnetization will relax to this position, with a characteristic damping coefficient α, the Gilbert damping (which can range between $\sim 5 \times 10^{-3}$ and 0.1 for standard ferromagnets, depending on the amplitude of their spin–orbit interactions). The damping force is once again associated with a torque, written

$$\left(\frac{d\vec{m}_2}{dt}\right)_{damping} = -\alpha \vec{m}_2 \times \frac{d\vec{m}_2}{dt}, \tag{1.19}$$

which tends to bring back $\vec{m}_2$ toward $\vec{H}_{eff}$ (Fig. 1.10).

1.3.2.1 A Simple Analogy
A simple analogy to understand the influence of STT on magnetization dynamics is the classical RLC resonant circuit. If the circuit is initially excited, for instance by introducing a charge on the capacity, the current in the circuit exhibits damped oscillations and gradually relaxes toward the zero equilibrium value. Because of dissipation, as long as no additional energy is supplied to the

system, it has no other choice but to relax to the closest equilibrium position. However, during this relaxation process, one can act on the system to modify the relaxation rate, by reducing or increasing the damping of the system. In the RLC analogy, this would correspond to adding a supplementary positive or negative resistance in the circuit. When dealing with magnetization, a means to do this is to use spin-transfer torque. Indeed, depending on the sign of the current, the resulting STT torque can be oriented either in the same direction or in the opposite direction to the damping torque.

This simplified description allows one to understand easily the nature of the main contribution of spin-transfer force (in-plane torque), which can be described through a non-conservative force acting in the same direction as the natural damping, that is, perpendicular to the magnetization trajectory. Depending on the relative orientation of $\vec{M}_1$ and $\vec{M}_2$, as well as the sign of the injected current, the spin-transfer torque can increase or decrease the effective damping, that is, behave as an additional damping or as an antidamping.

To continue the analogy with classical systems, like the RLC circuit, one can bring it into a regime where the effective damping around equilibrium crosses zero and becomes negative ($R_S < -R_0$). In this case, the corresponding equilibrium position is no longer stable, and any deviation from equilibrium is amplified so that the oscillations diverge. For the case of unstable local magnetization, thermal excitations are sufficient to induce a small deviation from equilibrium, further amplified by spin-transfer torque. Depending on the system configuration, the magnetic system can be designed so that the oscillation divergence drives the magnetization toward another stable minimum of energy or so that steady state excitations of the magnetization can be sustained. The first behavior is the one used to write in STT-MRAM, whereas the second behavior can yield to new types of frequency-tunable RF oscillators.

1.3.2.2 Toward MRAM Based on Spin-Transfer Torque

A STT-MRAM cell is effectively composed of a MTJ consisting of a pinned ferromagnetic reference layer and a ferromagnetic storage layer separated by a tunnel barrier. This system is very similar to the one described in Fig. 1.8 where the storage layer is F2 and the reference layer is F1. The MTJ is designed in such a way that the magnetization of the storage layer has two natural equilibrium positions parallel or antiparallel to the pinned layer magnetization. Using the spin-transfer torque to destabilize either one of these positions, simply by choosing the sign of the current, it is possible to induce a reversal of the magnetization, and consequently switch the value of the memory cell. When electrons flow from the pinned layer to the storage layer, parallel alignment is favored. When electrons flow from the storage layer to the reference layer, antiparallel alignment is favored. To achieve the storage layer magnetization switching, the current density must exceed a certain threshold, which corresponds to the point where the Gilbert damping becomes balanced by the STT antidamping. This current density threshold J_c can be calculated by finding the conditions for which the net effective damping is zero. The expression of the current density for switching depends in particular on whether the layers are magnetized in-plane or out-of-plane. This will be explained in more details in

Chapter 5. The LLG equation with Slonczewski in-plane torque yields the critical current density for switching:

$$J_c = \frac{2\alpha e \mu_0 M_S t}{\hbar P_{spin}} H_{eff},$$ (1.20)

and the corresponding critical current:

$$I_c = \frac{2\alpha e \mu_0 M_S V}{\hbar P_{spin}} H_{eff},$$ (1.21)

where M_s is the saturation magnetization, α is the Gilbert damping, t is the layer thickness, V is the volume, P_{spin} is the amplitude of the spin polarization, and H_{eff} is the effective field as previously defined. The other quantities are physical constants: e the electron charge, μ_0 the vacuum permeability, and $\hbar$ the reduced Planck constant. The predicted critical current densities are relatively large, in the range of a few 10^{11} A/m^2 in metallic spin valves and in the range of 1 to a few 10^{10} A/m^2 in MTJs. The higher STT efficiency in MTJs is associated with two phenomena: a higher spin polarization in particular in MgO-based MTJs, and the fact that in a MTJ, electrons impinging on the storage layer have mainly a perpendicular component of momentum. The electrons that tunnel the most easily through the barrier are those propagating perpendicular to the layers (with out-of-plane momentum $\vec{k} \approx \vec{k}_\perp$, $k_\parallel \approx 0$), whereas in metallic pillars, the electron momentum is broadly dispersed in all angular direction.

Very importantly for STT-MRAM considerations, STT switching is determined by a current density threshold. This means that the current required to write in STT-MRAM scales proportionally to the area of the device. For very small dimensions, for which thermal stability becomes a problem, a reduction in size must be compensated by an increase in the anisotropy field (and in H_{eff}) to maintain a desired thermal stability factor, that is, a given memory retention (see Chapter 5). As a consequence, the thermal stability limits the decrease of the critical current with the device dimensions. However, this minimum current value is in the range of 13 μA with known materials, which allows downsize scalability of STT-MRAM to sub-20 nm nodes.

The expression of critical current density provides paths to reduce the power consumption for spin-transfer-induced switching. In particular the Gilbert damping factor α plays a quite important role and must be minimized, and the spin polarization must be maximized. The other parameters (t, M_s, H_{eff}) also influence the thermal stability of the magnetization, so a trade-off must often be found between minimizing the write current density and maintaining sufficient thermal stability to achieve the specified memory retention. The goal of minimizing the critical current for writing has stimulated a strong research effort in the last few years, notably among two families of materials: magnetic oxides (26) and Heusler alloys (27).

1.3.3   Main Events Concerning Spin-Transfer Advances

A complete review of all the theoretical and experimental advances made in the last decade on spin-transfer is beyond the scope of this chapter (see Ref. 28 and references therein). However, it is worth mentioning a few key dates in spin-transfer torque research and development. The first experimental results to validate the

theoretical prediction of spin-transfer torque made by Slonczewski and Berger were obtained by Tsoi et al, using a point-contact geometry for injection of a large current density into a magnetic layer (29). The experimental demonstration of the use of spin-transfer torque to reverse the magnetization of metallic spin valves without any applied field by Katine et al. in 2000 (30) showed that STT could be used as a new write scheme in MRAM instead of field-induced magnetization switching, offering a much better downsize scalability. The first demonstration of STT switching in MTJs was made in 2004 (31) once the quality of the MTJ growth became good enough to withstand the large current density required for STT switching. The first functional demonstrator of an STT-MRAM chip was developed by Sony Corp, which presented the first 4 kbit STT-RAM demonstrator in 2004 (32). A lot of further progress has been made since then on both the fundamental understanding of the STT effects as well as on the technological side (see Chapter 6). The first STT-MRAM products were announced by Everspin at the end of 2012 (see Chapter 5) and all the major microelectronic companies now have large research and development efforts, in particular aiming at DRAM replacement by STT-MRAM beyond the 20 nm technological node.

REFERENCES

1. M. Baibich, J. M. Broto, A. Fert, F. Nguyen Van Dau, F. Petroff, P. Etienne, G. Creuzet, A. Friederch, and J. Chazelas, "Giant magnetoresistance of (001)Fe/(001)Cr magnetic superlattices," *Phys. Rev. Lett.* **61**, pp. 2472–2475 (1988); doi: 10.1103/PhysRevLett.61.2472.

2. J. S. Moodera, L. R. Kinder, T. M. Wong, and R. Meservey, "Large magnetoresistance at room temperature in ferromagnetic thin film tunnel junctions," *Phys. Rev. Lett.* **74**, pp. 3273–3276 (1995); doi: 10.1103/PhysRevLett.74.3273.

3. T. Miyazaki and N. Tezuka, "Giant magnetic tunneling effect in Fe/Al$_2$O$_3$/Fe junction," *J. Magn. Magn. Mater.* **139**, pp. L231–L234 (1995); doi: 10.1016/0304-8853(95)90001-2.

4. S. Tehrani, J. M. Slaughter, E. Chen, M. Durlam, J. Shi, and M. DeHerrera, "Progress and outlook for MRAM technology," *IEEE Trans. Magn.* **35**, pp. 2814–2819 (1999); doi: 10.1109/20.800991.

5. I. A. Campbell and A. Fert, "Transport properties of ferromagnets," in *Ferromagnetic Materials*, Vol. 3, ed. E. P. Wohlfarth, North-Holland Publishing, Amsterdam, 1987, pp. 747–804.

6. A. Barthélémy, A. Fert, and F. Petroff, "Giant magnetoresistance of magnetic multilayers," in *Handbook of Magnetic Materials*, Vol. 12, ed. K. H. J. Buschow, North-Holland, Amsterdam, 1999, pp. 1–96.

7. T. Valet and A. Fert, "Theory of the perpendicular magnetoresistance in magnetic multilayers," *Phys. Rev. B* **48**, pp. 7099–7113 (1993); doi: 10.1103/PhysRevB.48.7099.

8. S. S. P. Parkin, N. More, and K. P. Roche, "Oscillations in exchange coupling and magnetoresistance in metallic superlattice structures: Co/Ru, Co/Cr, and Fe/Cr," *Phys. Rev. Lett.* **64**, pp. 2304–2307 (1990); doi: 10.1103/PhysRevLett.64.2304.

9. B. Dieny, V. S. Speriosu, S. S. P. Parkin, B. A. Gurney, D. R. Wilhoit, and D. Mauri, "Giant magnetoresistance in soft ferromagnetic multilayers," *Phys. Rev. B* **43**, pp. 1297–1300 (1991); doi: 10.1103/PhysRevB.43.1297.

10. B. Dieny, "Spin valves," in *Magnetoelectronics*, ed. M. Johnson, Elsevier, Amsterdam, 2004, pp. 67–150.

11. M. Jullière, "Tunneling between ferromagnetic films," *Phys. Lett.* **54A**, pp. 225–226 (1975); doi: 10.1016/0375-9601(75)90174-7.

12. S. Yuasa, T. Nagahama, A. Fukushima, Y. Suzuki, and K. Ando, "Giant room-temperature magneto-resistance in single-crystal Fe/MgO/Fe magnetic tunnel junctions," *Nat. Mater.* **3**, pp. 868–871 (2004); doi: 10.1038/nmat1257.

13. S. S. P. Parkin, C. Kaiser, A. Panchula, P. M. Rice, B. Hughes, M. Samant, and S-H. Yang, "Giant tunnelling magnetoresistance at room temperature with MgO(100) tunnel barriers," *Nat. Mater.* **3**, pp. 862–867 (2004); doi: 10.1038/nmat1256.

14. R. Meservey and P. M. Tedrow, "Spin-polarized electron tunneling," *Phys. Rep.* **238**, pp. 173–243 (1994); doi: 10.1016/0370-1573(94)90105-8.

15. J. M. De Teresa, A. Barthélémy, A. Fert, J. P. Contour, F. Montaigne, and P. Seneor, "Role of metal-oxide interface in determining the spin polarization of magnetic tunnel junctions," *Science* **286**, pp. 507–509 (1999); doi: 10.1126/science.286.5439.507.

16. J. Slonczewski, "Conductance and exchange coupling of two ferromagnets separated by a tunneling barrier," *Phys. Rev. B* **39**, pp. 6995–7002 (1989); doi: 10.1103/PhysRevB.39.6995.

17. S. Yuasa and D. D. Djayaprawira, "Giant tunnel magnetoresistance in magnetic tunnel junctions with a crystalline MgO(001) barrier," *J. Phys. D Appl. Phys.* **40**, pp. R337–R354 (2007); doi: 10.1088/0022-3727/40/21/R01.

18. W. H. Butler, X.-G. Zhang, T. C. Schulthess, and J. M. MacLaren, "Spin-dependent tunneling conductance of Fe/MgO/Fe sandwiches," *Phys. Rev. B* **63** 054416 (2001); doi: 10.1103/PhysRevB.63.054416.

19. J. Mathon and A. Umerski, "Theory of tunneling magnetoresistance of an epitaxial Fe/MgO/Fe (001) junction," *Phys. Rev. B* **63**, 220403 (2001); doi: 10.1103/PhysRevB.63.220403.

20. J. P. Velev, K. D. Belashchenko, D. A. Stewart, M. van Schilfgaarde, S. S. Jaswal, and E.Y. Tsymbal, "Negative spin polarization and large tunneling magnetoresistance in epitaxial Co/SrTiO3/Co magnetic tunnel junctions," *Phys. Rev. Lett.* **95**, 216601 (2005); doi: 10.1103/PhysRevLett.95.216601.

21. S. Ikeda, J. Hayakawa, Y. Ashizawa, Y. M. Lee, K. Miura, H. Hasegawa, M. Tsunoda, F. Matsukura, and H. Ohno, "Tunnel magnetoresistance of 604% at 300 K by suppression of Ta diffusion in CoFeB/MgO/CoFeB pseudo-spin-valves annealed at high temperature," *Appl. Phys. Lett.* **93**, 082508 (2008); doi: 10.1063/1.2976435.

22. J. C. Slonczewski, "Current-driven excitation of magnetic multilayers," *J. Magn. Magn. Mater.* **159**, pp. L1–L7 (1996); doi: 10.1016/0304-8853(96)00062-5.

23. L. Berger, "Emission of spin waves by a magnetic multilayer traversed by a current," *Phys. Rev. B* **54**, pp. 9353–9358 (1996); doi: 10.1103/PhysRevB.54.9353.

24. M. D. Stiles and J. Miltat, "Spin-transfer torque and dynamics," in *Spin Dynamics in Confined Magnetic Structures III*, Topics in Applied Physics, Vol. 101, eds B. Hillebrands and A. Thiaville, Springer, pp. 225–308 (2006); doi: 10.1007/10938171_7.

25. S. C. Oh, S. Y. Park, A. Manchon, M. Chshiev, J. H. Han, H. W. Lee, J. E. Lee, K. T. Nam, Y. Jo, Y. C. Kong, B. Dieny, and K. J. Lee, "Bias-voltage dependence of perpendicular spin-transfer torque in asymmetric MgO-based magnetic tunnel junctions," *Nat. Phys.* **5**, pp. 898–902 (2009); doi: 10.1038/nphys1427.

26. M. Bibes and A. Barthélémy, "Oxide spintronics," *IEEE Trans. Electron Dev.* **54**, pp. 1003–1023 (2007); doi: 10.1109/TED.2007.894366.

27. T. Graf, C. Felser, and S. S. P. Parkin, "Simple rules for the understanding of Heusler compounds," *Prog. Solid State Chem.* **39**, pp. 1–50 (2011); doi: 10.1016/j.progsolidstchem.2011.02.001.

28. D. C. Ralph and M. D. Stiles, "Spin-transfer torques," *J. Magn. Magn. Mater.* **320**, pp. 1190–1216 (2008); doi: 10.1016/j.jmmm.2007.12.019.

29. M. Tsoi, A. G. M. Jansen, J. Bass, W. C. Chiang, M. Seck, V. Tsoi, and P. Wyder, "Excitation of a magnetic multilayer by an electric current," *Phys. Rev. Lett.* **80**, pp. 4281–4284 (1998); doi: 10.1103/PhysRevLett.80.4281.

30. J. A. Katine, F. J. Albert, R. A. Buhrman, E. B. Myers, and D.C. Ralph, "Current-driven magnetization reversal and spin-wave excitations in Co/Cu/Co pillars," *Phys. Rev. Lett.* **84**, pp. 3149 (2000); doi: 10.1103/PhysRevLett.84.3149.

31. Y. Huai, F. Albert, P. Nguyen, M. Pakala, and T. Valet, "Observation of spin-transfer switching in deep submicron-sized and low-resistance magnetic tunnel junctions," *Appl. Phys. Lett.* **84**, pp. 3118–3120 (2004); doi: 10.1063/1.1707228.

32. M. Hosomi, H. Yamagishi, T. Yamamoto, K. Bessho, Y. Higo, K. Yamane, H. Yamada, M. Shoji, H. Hachino, C. Fukumoto, H. Nagao, and H. Kano, "A novel nonvolatile memory with spin-torque transfer magnetization switching: Spin-RAM," IEEE International Electron Devices Meeting, IEDM Technical Digest, December 5–7, 2005, Washington, DC, pp. 459–462; doi: 10.1109/IEDM.2005.1609379.